Accepted Manuscript

International Journal of Modern Physics C

Article Title:	The experimental and numerical study of formation and collapse processes of ventilated supercavitating flow
Author(s):	Hossein Ali Kamali, Mohammad-Reza Erfanian
DOI:	10.1142/S0129183124502000
Received:	11 May 2024
Accepted:	25 June 2024
To be cited as:	Hossein Ali Kamali, Mohammad-Reza Erfanian, The experimental and numerical study of formation and collapse processes of ventilated supercavitating flow, *International Journal of Modern Physics C*, doi: 10.1142/S0129183124502000
Link to final version:	https://doi.org/10.1142/S0129183124502000

World Scientific
www.worldscientific.com

The experimental and numerical study of formation and collapse processes of ventilated supercavitating flow

Hossein Ali Kamali[a], *Mohammad-Reza Erfanian*[a] *

a Department of Mechanical Engineering, Ferdowsi University of Mashhad, Mashhad, Iran

ABSTRACT

The aim of this paper is to investigate the ventilated cavitating flow behavior, through experimental and numerical method. The experiments are performed for a test-model placed in a water tunnel and a high-speed camera is used to image the formation and collapse of the supercavity. For the numerical simulations, Ansys CFX commercial software is employed to solve the Reynolds Averaged Navier Stokes (RANS) equations and additional transport equation for the liquid volume fraction in the unsteady condition. Both the experimental observation and numerical prediction show a hysteresis behavior for ventilated supercavity in which the value of air entrainment coefficient required to maintain the supercavity in the formation process is less than the amount required to form it. The good agreement observed between the numerical prediction and experimental data, revealed the accuracy and capability of the numerical scheme. Also, the numerical simulation shows that the variations in the supercavity length, in addition to the air entrainment, are a function of air leakage regime from the closure region of supercavity.

Keywords: Cavitating flow; Supercavity length; Hysteresis behavior; Formation process; collapse process; closure region.

PACS number: 44.35.+c

NOMENCLATURE

C_q	air entrainment coefficient	U_∞	free-stream velocity
C_{qc}	critical air entrainment in collapse process	$\dot{Q}$	air flow rate
C_{qf}	critical air entrainment in formation process	ρ	density
D_n	cavitator diameter	μ	viscosity
L	supercavity length	α	volume of fluid

1. INTRODUCTION

Supercavitation is one of the effective technology to reduce the drag force of underwater bodies. In the cavitating flow, all or most of the body surface is covered by a non-condensable gas, and its drag force is significantly reduced [1]. Supercavitation is of two types: natural and ventilated. In the natural supercavitation, the speed of the underwater vehicle needs to be increased to a large value (about 100 m/s) and areas where the pressure is lower than the saturation pressure to encompass the body [2]. This method is almost non-applicable, especially for large vehicle such as projectiles and submarines. In the ventilated cavitation, air is injected to the underwater vehicle to cover the body surface. The ventilated supercavitation is a successful method to reducing the frictional drag force of moving and submerged bodies in water [3]. The most important non-dimensional parameter used in the ventilated cavitation is the air entrainment coefficient (Cq), which is defined as:

$$C_q = \frac{\dot{Q}}{D_n^2 U_\infty} \quad (1)$$

where $\dot{Q}$ is the volumetric flow rate of the injected air, D_n is the cavitator diameter and U_∞ is the free stream velocity.

Research studies on the phenomenon of ventilated supercavitation have increased dramatically in recent years because of its request to reducing the drag force of submerged bodies and achieving high velocities. The characteristics and behavior of ventilated supercavitation have been investigated have been studied by many researchers using analytical, experimental, and numerical approaches. Early research in this field is devoted mostly to extracting

* Corresponding author.
E-mail address: mohammad.erfanian09@gmail.com.

empirical or semi-empirical relationships to determine the size of the natural supercavity. In the last decade, the development of CFD (computational fluid dynamics) techniques and also the accessibility of the advanced computers, have led most researchers to study on cavitating flows using numerical simulation [4]. Although, through experimental observations, some features of cavitating flow have been revealed, but some of its flow complexities remain unknown, which can be studied by numerical simulation [5]. In recent years, most studies have investigated the amount of air required to form a stable supercavity. In the following paragraphs, the most remarkable works about the cavitating flow are reviewed.

Zhang et al. [6] employed an experimental method to compare the natural and ventilated supercavity shape around a test object and studied the flow field structures. Bin et al. [7] simulated natural and ventilated cavitating flows around a model using the assumption of homogeneous mixture model (which considers the two-phase mixture to be a single fluid with pseudo properties). Kawakami and Arndt [8] investigated the ventilated cavitating flow around a disk-shaped cavitator subjected in water tunnel and studied the supercavity shape, re-entrant mechanism (periodic cloud shedding in partial cavitation) at closure region and effect of the air entrainment coefficients on supercavity behavior. Wang et al. [9] experimentally and numerically studied the ventilated cavitating flow pattern around a model. The results show that with the increasing of the C_q in the formation process, there was a critical value in which the cavity dimensions increased considerably and then remain constant. Karn et al. [10,11] investigated the different closure mechanism of ventilated supercavity in the formation and collapse processes over a wide range of blockage ratios and Froude numbers. Kamali et al. [12] studied the effect of the cavitator angle in different ventilation coefficient on the cavity characteristics. Sun et al. [13] experimentally investigated the unstable conditions of a ventilated supercavity at the closure region in the formation process. Xu et al. [14] explored the evolution of supercavity geometry and the transient characteristics of supercavitation flow from initial formation to full development for different air entrainment coefficients and Froude numbers. Xu et al. [15] investigated the effects of the air entrainment and supersonic gas jet. They analyzed the mechanism of supercavity-jet interactions with the air leakage rate. Moltani et al. [16] studied the effect of free surface condition on ventilated supercavity formed around the surface vehicle, experimentally and numerically.

Despite many studies in this area, the supercavity collapse process and the hysteresis behavior of ventilated supercavitation have received less attention. The above-mentioned studies have generally investigated half of the hysteresis map (formation process line). The aim of this study is to investigate the effect of the air entrainment rate on the supercavity dimensions and the air leakage regime of the closure region in formation stage of the supercavity and its collapse stage. The calculation of critical air entrainment coefficients and hysteresis map are very important in the design of the gas supply system of an underwater device, which are determined in this paper. Also, the reason for supercavity dimensions changes in the formation and collapse stages is studied by numerical simulation.

2. Experimental Method

In order to experimentally study the supercavitating flow in the present work, the closed-circuit water tunnel of Iran University of Science and Technology and its related equipment was used. This water tunnel has a test-section with length of 2m, width of 0.1m, and height of 0.2m, which is shown in Fig. 1. The centrifugal flow pump (70 HP and 500 m^3/hr) is used to circulate water in the tunnel with velocities of 5-9 m/s. An electromagnetic flow meter is used to measure the water flow rate (Endress+Hauser Flowtec model); also, the volumetric of injected air is measured by means of a glass rotameter LZB-3WB and LZB-4WB (The reported errors for both flowmeters are about4%.). The air injection system includes a compressed air compressor and a pressure regulating valve that is injected into the test model through the pipe. The air injection equipment is presented in Fig. 2. The test model depicted in Fig. 3, has a disk- cavitator with diameter of 10 mm and cylindrical main body with diameter of 20 mm. The test model length is L=375 mm. A high-speed photographic camera is employed to capture the supercavity. around the model.

Fig. 1. The water tunnel of Iran University of Science and Technology

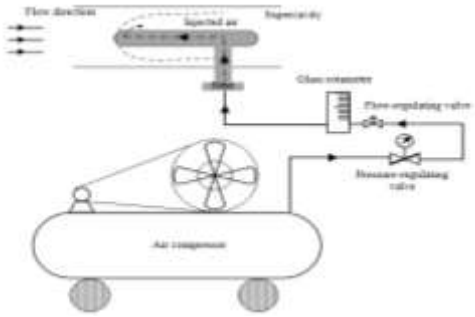

Figure 2- The air injection system

Fig. 3- The test-model placed in the test section of water tunnel

3. MATHEMATICAL MODELING

3.1 Governing Equations

In the current study, the Reynolds-averaged Navier–Stokes equations are employed to simulate the supercavitating flow, in which the fluid is considered as a homogeneous mixture of liquid (water) and a non-condensable gas (air). The governing multiphase flow equations containing of the continuity and momentum are:

$$\frac{\partial \rho}{\partial t}+\frac{\partial(\rho u_j)}{\partial x_j}=0 \tag{2}$$

$$\frac{\partial(\rho u_i)}{\partial t}+\frac{\partial\left(\rho u_i u_j\right)}{\partial x_j}=\rho f_i-\frac{\partial p}{\partial x_j}+\frac{\partial}{\partial x_j}\left[(\mu+\mu_t)\left(\frac{\partial u_i}{\partial x_j}+\frac{\partial u_j}{\partial x_i}-\frac{2}{3}\frac{\partial u_k}{\partial x_k}\delta_{ij}\right)\right] \tag{3}$$

u_i, p, and f_i represent the velocity, pressure and body force in ith direction, respectively. ρ is the mixture density and μ is the mixture viscosity, which are considered with linear function of volume fraction [17]:

$$\rho=\alpha_v\rho_v+(1-\alpha_v)\rho_l \tag{4}$$

$$\mu=\alpha_v\mu_v++(1-\alpha_v)\mu_l \tag{5}$$

where α is the phase volume fraction. The subscripts l and a show the liquid and gas phases, respectively. the transport equation of liquid volume fraction is considered as:

$$\frac{\partial(\alpha_a\rho_a)}{\partial t}+\frac{\partial\left(\alpha_a\rho_a u_j\right)}{\partial x_j}=\nabla.\left(\frac{\Gamma_a\nabla\alpha_a\rho_a}{\rho}\right) \tag{6}$$

The liquid volume fraction, α_l, and the gas volume fraction, α_a, are:

$$\alpha_l=\frac{liquid\ volume}{total\ volume} \qquad \alpha_l=\frac{air\ volume}{total\ volume}$$

$$\alpha_l+\alpha_v=1 \tag{7}$$

3.2 Turbulence Modeling

The *k-ω* SST turbulence model presented by Menter [18] is generally used two-equation eddy-viscosity turbulence model [19]. The accuracy of the *k-ω* SST model for multi-phase flow is revealed in various studies [20-25]. In this model, the turbulence kinetic energy (k) and the rate of dissipation of eddies (ε), are:

$$\frac{\partial(\rho k)}{\partial t}+\frac{\partial\left(\rho u_j k\right)}{\partial x_j}=P-\beta^*\rho\omega k+\frac{\partial}{\partial x_j}\left[(\mu+\sigma_k\mu_t)\frac{\partial k}{\partial x_j}\right] \tag{8}$$

$$\frac{\partial(\rho\omega)}{\partial t}+\frac{\partial\left(\rho u_j\omega\right)}{\partial x_j}=\frac{\gamma}{v_t}P-\beta^*\rho\omega^2+\frac{\partial}{\partial x_j}\left[(\mu+\sigma_\omega\mu_t)\frac{\partial\omega}{\partial x_j}\right]+2(1-F_1)\frac{\rho\sigma_{\omega2}}{\omega}\frac{\partial k}{\partial x_j}\frac{\partial\omega}{\partial x_j} \tag{9}$$

where τ_{ij} is the shear stress tensor, and P is:

$$P=\tau_{ij}\frac{\partial u_i}{\partial x_j} \tag{10}$$

$$\tau_{ij}=\mu_t\left(2S_{ij}-\frac{2}{3}\frac{\partial u_k}{\partial x_k}\delta_{ij}\right)-\frac{2}{3}\rho k\delta_{ij} \tag{11}$$

$$S_{ij}=\frac{1}{2}\left(\frac{\partial u_i}{\partial x_j}+\frac{\partial u_j}{\partial x_i}\right) \tag{12}$$

and the turbulent eddy viscosity is calculated from:

$$\mu_t=\frac{\rho a_1 k}{\max(a_1\omega,\Omega F_2)} \tag{13}$$

Each parameter in the SST k-ω model is a linear blend of the corresponding constants of k-ω and k-ε turbulence models, which are defined:

$$\phi=F_1\phi_1+(1-F_1)\phi_2 \tag{14}$$

where Φ_1 denotes *k-ω* constants and Φ_2 represents the *k-ε* constants. Additional functions are given by:

$$F_1=\tanh(arg_1^4) \tag{15}$$

$$arg_1=min\begin{bmatrix}max\left(\frac{\sqrt{k}}{\beta^*\omega h},\frac{500v}{h^2\omega}\right)\\ \frac{4\rho\sigma_{\omega2}k}{CD_{k\omega}h^2}\end{bmatrix} \tag{16}$$

$$CD_{k\omega}=max\begin{pmatrix}2\rho\sigma_{\omega2}\frac{1}{\omega}\frac{\partial k}{\partial x_j}\frac{\partial\omega}{\partial x_j}\\ 10^{-20}\end{pmatrix} \tag{17}$$

$$F_2=\tanh(arg_2^2) \tag{18}$$

$$arg_2=max\left(2\frac{\sqrt{k}}{\beta^*\omega d},\frac{500v}{h^2\omega}\right) \tag{19}$$

3.3 Numerical Methods

In this study, the commercial CFD package Ansys CFX 15 was used to simulate the cavitating flow in three-dimensional and unsteady conditions around the test object. The finite volume method is applied in pressure-based conditions to convert the nonlinear equations into algebraic relations which are solvable by numerical methods. The (SIMPLE) algorithm is also considered for the relation between pressure and velocity. The viscosity and density of water are assumed to be ρ_l=998 kg/m^3 and μ_l=1.140×10^{-3} Pa.s, respectively, which correspond to the properties of pure water at 25 ° C. The density of the injected air is ρ_a=1.185 kg/m^3 and the viscosity is μ_a=1.830×10^{-5} Pa.s.

In the numerical simulation, the test model used in the experiments is considered. The computational domain dimensions and model location are based on the water tunnel test section. A fixed value for velocity with volume fraction of 1 for water is considered for inlet boundary. Also, a fixed value for

pressure is applied to exit boundary condition. For the side, lower and upper surfaces of the domain as well as the model surface, the non-slip wall boundary is used. To vent the air around the body, a fixed value for air mass flow rate with volume fraction of 1 for air is applied to injection surface.

The computational domain is meshed with hexahedral cells using Ansys meshing 15 software. To ensure the quality of the grid, a mesh refinement study is performed in which the grid size is gradually reduced until no significant changes are seen in the simulation results. In order to specify the mesh-independent grid, the dimensionless supercavity length, L/D_n, obtained using three different grid sizes are presented in table 1. The results revealed that the medium grid with 1200000 computational cells is the most appropriate grid from the viewpoint of both the computational time and the numerical accuracy. The y^+ value on the surface of the model is less than 1. Fig. 4 shows the boundary condition and the mesh distribution around the test model for the medium grid. The required calculation time for each simulation is about 16 h, in the parallel form on 4 cores of Core i7-2600 CPU, 3.4 GHz

Table 1 Dimensionless supercavity length for different grid

Grid	L/D_n
Coarse	30.2
Medium	35.5
Fine	35.9

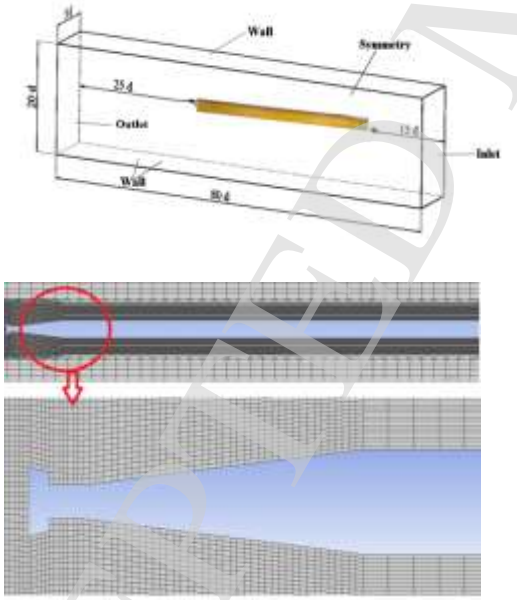

Fig. 4- The boundary condition and the mesh distribution around the test-model for medium grid

4. RESULTS AND DISCUSSION

In this paper, the ventilated cavitating flow around the disk cavitator body with special emphasis on the hysteresis behavior of the supercavity is investigated through the experimental and numerical techniques. The experimental observations obtained through the water tunnel equipment on a disk cavitator body. The numerical simulations of the cavitating flow were performed using the commercial CFD software Ansys CFX 15.

In the experimental observations, the air flow rate is gradually increased (named formation process) and after reaching the maximum value, we continuously reduce the air flow rate (named collapse process) until the formed supercavity disappears. After each step of increase or decrease, airflow is recorded in a table and high-speed photography of cavitating flow is performed. Fig. 5 shows the supercavity images in the formation process at Fr= 23.5. The air entrainment coefficient and corresponding supercavity length were also recorded in the figure. As shown in the figure, with the increase of C_q, the supercavity length is continuously increased and the supercavity becomes clearer. With the increase of air entrainment coefficient to Cq = 0.046 (case 8), a sudden increase in supercavity dimensions is observed, and further increase entrainment coefficient to Cq = 0.075 (case 11) does not considerably increase the supercavity length.

After reaching the maximum length of supercavity in the formation process, we gradually reduce the air flow rate to initiate the collapse process. Fig. 6 shows the supercavity images in the collapse process at Fr= 23.5. It can be seen from the figure, by decreasing the C_q to 0.037 (case 3), no significant reduction in supercavity dimension occurs. It is noteworthy that at the collapse stage, the supercavity size remains almost constant with a 50% decrease in the air entrainment coefficient. Finally, with a further decrease in the air entrainment to C_q = 0.031 (case 4), a sharp drop in the supercavity dimensions occurs and supercavity collapses. Consequently, a supercavity can be preserved at a lower air entrainment value in the collapse stage than is required to form it. This difference between the C_q values in the formation and collapse stages (C_q=0.05 in the formation stage vs. C_q=0.037 in the collapse stage) indicates the existence of hysteresis behavior for ventilated supercavity.

Fig.7 represents the hysteresis curve (air entrainment coefficient vs. supercavity length) at the Fr=23.5. The figure shows, in the formation stage, as the C_q increases, the supercavity length is also increased. With the further increase in C_q, the supercavity length increases significantly against the slight increase in C_q to reach the its critical value (C_{qf}), which is shown by ((a)) in the fig.7. With further increase in the C_q greater than C_{qf}, the supercavity size does not increase significantly and remains almost constant. In the collapse stage, the supercavity length is resistant to the decrease in C_q and does not reduce significantly.

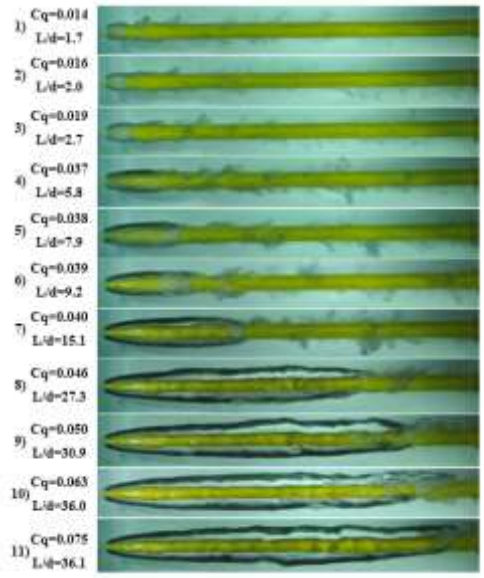

Fig. 5- The supercavity images in the formation process at *Fr*=23.5

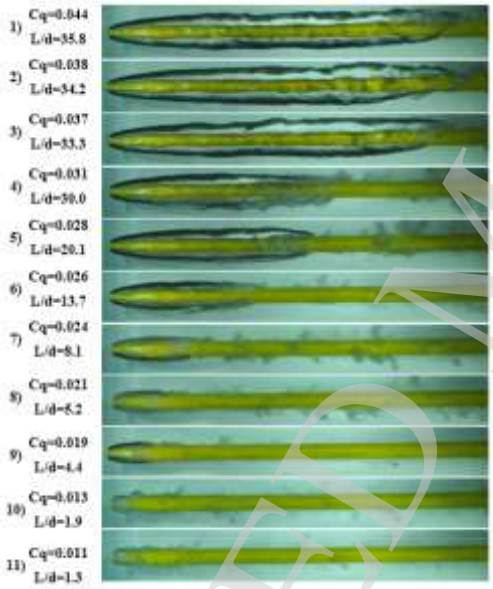

Fig. 6- The supercavity images in the collapse process at *Fr*=23.5

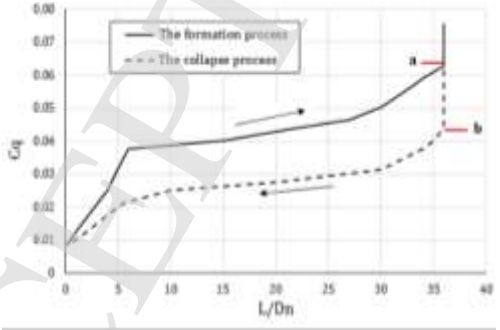

Fig. 7- The hysteresis curve (C_q vs. L/D_n) for ventilated supercavity at Fr=23.5

Further reduction of C_q to values less than the critical air entrainment coefficient, C_{qc}, will lead to a sharp decrease in supercavity length. The critical value of C_q in the collapse stage is shown by ((*b*)) in the fig.7. Therefore, the volume of air needed to have a proper supercavity is in the range between C_{qc} and C_{qf}. To investigate the cause of the supercavity length variations, which are mainly due to the air leakage pattern from the closure region of the supercavity [26,27], the ventilated cavitating flow is studied by numerical simulation. First, to ensure the accuracy of the numerical simulation, the numerical results are compared with the experimental observations and their accuracy is revealed. Fig. 8 compares the supercavity images obtained from the simulation results at different C_q with those of obtained experimentally. The good agreement between the numerical results and experimental photography indicates the ability of the numerical methodology to simulate the cavitating flow with a good accuracy. The air leakage pattern from the supercavity closure region is depicted in Fig. 9. The figure shows, at low values of air entrainment (C_q = 0.023) in the formation stage, the re-entrant jet mechanism is the dominant at the supercavity closure. In this mechanism, in which the air leakage from the supercavity is difficult, occurs when the pressure difference inside and outside the supercavity (ΔP) is large. As the C_q increases, the pressure inside the cavities increases, resulting in a decrease in the pressure difference.

With further increase in C_q, ΔP is reduced to a critical value that is no longer able to maintain the re-entrant jet regime and the air leakage pattern from the supercavity closure becomes twin vortex regime, in which, the air leakage form the supercavity is easier than the re-entrant jet regime. In the twin vortex regime, the air leakages through the large bubble packages. Therefore, in the re-entrant turn jet regime where air leakages with difficulty from the supercavity closure region, the increase in the air entrainment leads to an increase in the supercavity length. On the other hand, in the twin vortex mechanism where air easily leakages from the supercavity closure region, the increase in the air entrainment will not result in a significant increase in supercavity length.

In the collapse stage, at first, by reducing the air entrainment, ΔP is not large enough to re-establish a re-entrant jet regime, and thus the twin vortex regime (up to the C_q=0.035) remains. As the air entrainment coefficient decreases further to the critical value, C_{qc}, the pressure inside the supercavity will decrease, and the pressure difference inside and outside of the supercavity will increase. As a result, the twin vortex regime is replaced by re-entrant jet regime and the supercavity length will be greatly reduced.

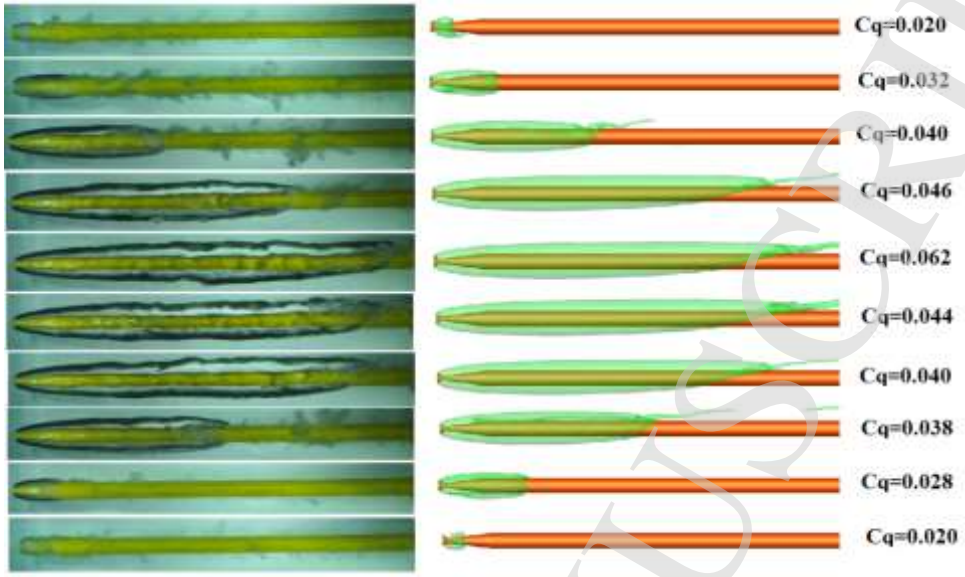

Fig. 8- Comparing numerical results with experimental photographs for supercavity shape

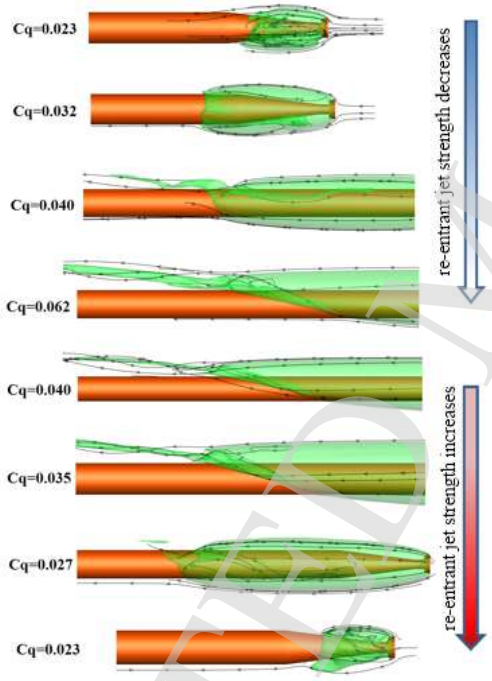

Fig. 9. The variations of air leakage regime at closure region of supercavity

5. CONCLUSION

In this study, the ventilated supercavitating flow around a cavitator disk object is studied using the experimental observations and computational fluid dynamics. For experimental observations, the water tunnel system of Iran University of Science and Technology was used, and to solve the governing equations of ventilated cavitating flow the Ansys CFX commercial software was employed. The numerical results were compared with the experimental results and good agreement was observed. Based on the experimental results and numerical simulation data, the following results were obtained:

1- With the gradual increase of C_q (in the formation stage), the cavity length of is first slightly increased and then with a small increase in C_q, the supercavity length will increase sharply. Then, with the further increase in the C_q, the supercavity length will not change considerably.

2- By gradually decreasing the C_q (in the collapse process), the supercavity length does not decrease significantly. But with the further decrease of C_q to a critical value, the supercavity length is significantly reduced and supercavity collapses.

3- The variation of the air entrainment coefficient versus the supercavity length shows a hysteresis behavior for ventilated supercavity behavior.

4- Changes in supercavity length versus the air entrainment coefficient are due to changes in the air leakage regime at the closure region of supercavity. At low values of C_q, where the pressure difference inside and outside the supercavity is high, the re-entrant jet regime is dominant. By increasing C_q, the pressure difference decreases and then the twin vortex regime is replaced at the closure region of supercavity.

REFERENCES

[1] K. Seon-Hong, K. Nakwan, Hydrodynamics and modeling of a ventilated supercavitating body in transition phase, J. Hydrodyn. Ser. B, vol.27 (5), pp. 763-772, 2015.

[2] M.-R. Erfanian. M. Anbarsooz, Numerical investigation of body and hole effects on the cavitating flow behind a disk cavitator at extremely low cavitation numbers, Applied mathematical modelling, vol. 62, pp. 163-180, 2018.

[3] Y.J. Wei, W. Cao, C. Wang, J.Z. Zhang, Z.Z. Zou, Experimental research on character of ventilated supercavity, in: Proceedings of the Fifth International Conference on Fluid Mechanics, Shanghai, China, 2007 Aug.15-19.

[4] S. Park, S. H. Rhee, Computational analysis of turbulent super-cavitating flow around a two-dimensional wedge-shaped cavitator geometry, Computers & Fluids, vol. 70, pp. 73-85, 2012.
[5] Z. Shang, Numerical investigations of supercavitation around blunt bodies of submarine shape, Applied Mathematical Modelling, Vol. 37, No. 20–21, pp. 8836-8845, 2013.
[6] X.-w. ZHANG, Y.-j. WEI, J.-z. ZHANG, W. Cong, K.-p. YU, Experimental research on the shape characters of natural and ventilated supercavitation, Journal of Hydrodynamics, Ser. B, vol. 19 (5), pp. 564-571, 2007.
[7] J. Bin, X.-W. Luo, X.-X. Peng, Y. Zhang, Y.-L. Wu, H.-Y. Xu, Numerical investigation of the ventilated cavitating flow around an under-water vehicle based on a three-component cavitation model, Journal of Hydrodynamics, Ser. B, Vol. 22, No. 6, pp. 753-759, 2010.
[8] E. Kawakami and R. Arndt, "Investigation of the Behavior of Ventilated Supercavities," Transactions of the ASME, Journal of fluid engineering, vol. 133, 2011.
[9] Z. Wang, B. Huang, G. Wang, M. Zhang and F. Wa, "Experimental and numerical investigation of ventilated cavitating flow with special emphasis on gas leakage behavior and re-entrant jet dynamics," Ocean Engineering, vol. 108, pp. 191-201, 2015.
[10] A. Karn, R.E. A. Arndt, J. Hong, Dependence of supercavity closure upon flow unsteadiness, Experimental Thermal and Fluid Science, vol. 68, pp. 493-498, 2015.
[11] A. Karn, R. E. A. Arndt, J. Hong, An experimental investigation into supercavity closure mechanisms, Journal of Fluid Mechanics, vol. 789, pp. 259-284, 2016.
[12] Kamali, H.A., M.-R. Erfanian, and M. Pasandidehfard, Experimental and numerical analysis of cavitator angle effects on artificial cavitation characteristics under low ventilation coefficients, with prediction using optimized random forest and extreme gradient boosting models. Ocean Engineering, 2024. 309: p. 118446.
[13] T. Sun, X. Zhang, Ch. Xu, G. Zhang, C. Wang, Zh. Zong, Experimental investigation on the cavity evolution and dynamics with special emphasis on the development stage of ventilated partial cavitating flow, Ocean Engineering 187, 106140, 2019.
[14] Haiyu Xu, Cong Wang, Yingjie Wei, Wei Cao, Wei Wang, On the evolution of supercavity geometry and unsteady behavior of supercavitation flow during the development of a twin-vortex supercavity, Ocean Engineering, Volume 276,2023,114213.
[15] Haiyu Xu, Cong Wang, Yingjie Wei, Wei Cao, Wei Wang, Analysis of the effect of underwater supersonic gas jet on the ventilated supercavitation flow, Ocean Engineering, Volume 299, 2024, 117278.
[16] Ali-Akbar Moltani, Mahmoud Pasandideh Fard, Mohammad-Reza Erfanian, Experimental and numerical study of free surface effect on the ventilated cavitating flow around a surface vehicle model, Ocean Engineering, Volume 268, 2023, 113413.
[17] B. Ji, X. Luo, Y. Wu, X. Peng, H. Xu, Numerical investigation of the ventilated cavitating flow around an under-water vehicle based on a three-component cavitation model, Journal of hydrodynamics, vol. 22 (6), pp. 753-759, 2010.
[18] F.R. Menter, Two-equation eddy-viscosity turbulence models for engineering applications, AIAA J., vol. 32 (8), pp. 1598–1605, 1994.
[19] H. Versteeg, W. Malalasekera, An Introduction to Computational Fluid Dynamics: The Finite Volume Method (2nd Edition), Pearson Education Limited, Prentice Hall, 2007.
[20] P. G. Huang, Physics and computations of flows with adverse pressure gradients, Modeling Complex Turbulent Flows, vol. 7, pp. 245-258, 1999.
[21] Godasiaei, S.H. and H. Kamali, Water jet angle prediction in supersonic crossflows: Euler–Lagrange and machine learning approaches. Eur. Phys. J. Plus, 2024. 139(3): p. 251.
[22] M. R. Pendar, E. Roohi, Investigation of cavitation around 3D hemispherical head-form body and conical cavitators using different turbulence and cavitation models, Ocean Engineering, vol. 112, pp. 287–306, 2016.
[23] Kamali, H.A., M. Pasandidehfard, and E. Kadivar, Analyzing the influence of dimensions of the body behind the cavitator on ventilated cavitation. Physics of Fluids, 2024. 36(6).
[24] Kamali, H.A., M. Pasandidehfard, and M.M. Rashidi, Effect of the arrangement of the injectors on the flow quantities in water injection into the hot supersonic crossflow inside the cylinder. International Journal of Modern Physics C. 0(0): p. 2450145.
[25] Kamali, H.A. and M. Pasandidehfard, Investigating the interaction parameters on ventilation supercavitation phenomena: Experimental and numerical analysis with machine learning interpretation. Physics of Fluids, 2023. 35(11).
[26] A. Karn, R. E. A. Arndt, J. Hong, An experimental investigation into supercavity closure mechanisms, Journal of Fluid Mechanics, Vol. 789, pp. 259-284, 2016.
[27] M.-R. Erfanian, M. Moghiman, Experimental investigation of critical air entrainment in ventilated cavitating flow for a forward-facing model, Applied Ocean research, Volume 97, 2020, 102089.